P1.5 **COMBINING SUB-FACET SCALE URBAN ENERGY BALANCE AND SENSOR VIEW MODELS TO INVESTIGATE THE DEPENDENCE OF EFFECTIVE THERMAL ANISOTROPY ON CITY STRUCTURE**

Scott Krayenhoff[1,*], James Voogt[2]
[1]University of British Columbia, Vancouver, Canada
[2]University of Western Ontario, London, Canada

1. INTRODUCTION

The urban surface energy balance drives urban climate and many urban boundary layer processes. Surface temperature is determined by the surface energy balance, and is related in a fundamental way to each of its component fluxes (with the exception of the solar forcing). Passive remote sensing of upwelling thermal radiance is an efficient means of observing the spatial distribution of urban surface temperature.

However, there are three primary causes of uncertainty in temperatures derived from remote sensing: (1) atmospheric absorption, emission and scattering between the surface and the sensor, (2) uncertainty in both surface emissivity and longwave radiation reflected from the surface, and (3) for remote sensors with limited fields of view (FOVs), sensitivity to variation in surface temperature, emissivity and reflected longwave radiation over the 3-D surface due to differences of the effective 3-D radiometric source area (i.e., the instantaneous FOV projected onto the surface) with viewing angle (Voogt and Oke 1998). The latter two causes of uncertainty in remotely-sensed temperature have received little attention; cause 3 in particular results in the directional brightness temperature (T_B), the temperature of a blackbody that would emit the same radiance as the radiance actually observed with a radiometer, differing with sensor viewing angle and direction. This effect is referred to as effective thermal anisotropy (Voogt and Oke 1998).

A few studies reporting effective anisotropy have been undertaken in urban areas (e.g. Voogt and Oke 1998; Lagouarde et al. 2004), but in order to isolate individual factors influencing effective anisotropy and to investigate the full range of each factor, modeling of both the complete energy balance and the viewing of the surface by the sensor is required. Here we explore the utility of the "Temperatures of Urban Facets in 3-D" (TUF-3D; Krayenhoff and Voogt 2007) energy balance model in the investigation of effective anisotropy when combined with the Surface-sensor-sun Urban Model (SUM; Soux *et al.*, 2004). Both models have been evaluated and shown to perform well (Krayenhoff and Voogt 2007; Soux et al. 2004).

Urban form is expected to be a strong control on effective anisotropy (Voogt and Oke, 1998). Therefore, this work focuses on the *daytime* evolution of effective anisotropy with varying λ_p, building aspect ratio (H/L), and street orientation (η). Modeling is done for clear skies and moderate to low wind speeds (mean of 2.0 m s^{-1}), atmospheric conditions for which effective anisotropy is expected to be maximized.

The current work is exploratory in nature, and the focus is on the links between urban form and effective anisotropy. To make it more relevant to urban climatologists, four of the urban land-use zones defined in Arnfield (1982), ranging from residential to industrial to modern high-rise commercial, are simulated to explore how effective anisotropy may be expected to vary across a city.

* *Corresponding author address*: Scott Krayenhoff, Univ. of British Columbia, Dept. of Geography, Vancouver, BC, V6T 1Z2; email: skrayenh@gmail.com

2. MEASURES OF EFFECTIVE ANISOTROPY

Given the preliminary nature of this work, identifying the bounds of effective thermal anisotropy (i.e. maximum differences) is the focus. Effective thermal anisotropy has typically been quantified as the maximum difference, or range, of a T_B distribution resulting from a chosen range of view directions (e.g. Voogt and Oke, 1998):

$$\Lambda = T_{B,\max} - T_{B,\min} \quad (1)$$

A supplementary measure is based on the use of the nadir temperature as a reference because the latter is the easiest to define and the most commonly used. The maximum difference from $T_{B,nad}$ is given by:

$$\Lambda_N = \max\left(T_{B,\max} - T_{B,nad}\,,\, T_{B,nad} - T_{B,\min}\right) \quad (2)$$

It is also useful to capture the daytime variation of Λ and Λ_N. For this purpose the daytime median (the temporal distributions of modeled hourly daytime Λ and Λ_N are usually not normal) and maximum hourly values are calculated, where daytime includes those hours for which the solar elevation angle is > 0º: e.g., Λ_{med}, $\Lambda_{\max}$.

3. MODEL COUPLING

TUF-3D is a dry, three-dimensional microscale urban energy balance model with the ability to simulate surface temperatures at the sub-facet scale for a variety of surface geometries and properties, weather conditions, and solar angles. All TUF-3D domains used here are composed of repeated 'urban units', which consist of one building or block surrounded by road (Krayenhoff and Voogt 2007). The surface temperatures from the central urban unit are extracted from TUF-3D output and replicated over an N by N array to provide an urban surface of sufficient size for viewing by a remote sensor, where N is the number of urban units. SUM is

then run for a number of different view angles. The brightness surface temperature as viewed by the sensor at each angle is determined using the Stefan Boltzmann relation (i.e., a broadband approximation).

SUM is set to sample the T_B distribution at regular intervals of the sensor off-nadir and azimuthal angles (0°-45° in 5° increments and 0°-350° in 10° increments, respectively). The remote sensor height is set so that it samples a representative portion of the surface while minimizing computation time. In its present implementation SUM views the intra-facet temperature variation, whereas its previous applications have been limited to sunlit and shaded facet-scale average temperature inputs from either direct observation or facet-averaged energy balance models, such as that of Mills (1997) (e.g. Voogt and Krayenhoff 2005).

4. SIMULATION DESIGN

TUF-SUM simulations are performed for a range of plane-parallel, regularly-spaced, aligned buildings with square footprints. $K\downarrow$ and $L\downarrow$ are calculated by TUF-3D internal routines assuming clear skies.

4.1 Variation of anisotropy with urban form

A suite of 486 24-hour TUF-3D simulations is performed for June 21 at latitude 47º 34' N (Basel) with all combinations of the variables λ_p, H/L and η. SUM is then run for every daylight hour, on the hour (in local mean solar time, or LMST). λ_p, H/L and η are varied according to Table 1, and together these parameters fully describe the variation of regularly-spaced, aligned arrays of identical square-footprint buildings. Radiative and thermal parameters are those for Basel-Sperrstrasse found in Krayenhoff and Voogt (2007).

4.2 Effective anisotropy of urban land use zones

As a more practical set of results, we present some case studies based on the urban land use zones for Columbus, Ohio defined in Arnfield (1982). Simulations are again for June 21 at the latitude of 47º 34' N. Realistic forcing is all that is required, since the intention of these simulations is to investigate the variation of effective anisotropy between typical urban land use zones.

Table 1: Geometric parameters for June 21 latitude 47º 34' N simulations. All possible combinations are simulated ($9\lambda_p \cdot 6$ $H/L \cdot 9$ $\eta = 486$ 1-day model runs).

Parameter	Approximate Values[1]
λ_p	0.06, 0.11, 0.20, 0.25, 0.31, 0.36, 0.41, 0.48, 0.54
H/L	0.4, 0.7, 1.0, 1.5, 2.0, 3.0
η	0° – 80° in 10° increments[2]

[1]Given the discrete nature of TUF-3D, values are within ±0.014 in λ_p and ±0.1 in H/L.

[2]This represents the full range of η variation due to symmetry.

The COM4, COM2, RES2 and IND land use zones of Arnfield (1982) are simulated here, representing modern high-rise commercial (22 storeys), built-up commercial (6-storeys), high density detached residential and light industry warehouse areas, respectively (Table 2). These land use zones fit into urban climate zones (UCZs) 1, 2, 3 and 4 of Oke (2006), respectively (Table 2). Geometric and radiative parameters and construction materials are extracted directly from Arnfield (1982). Roofs are tar-gravel; streets are asphalt with some concrete; walls are mixed brick, stone and wood siding for RES2, brick for IND, brick, concrete and stone for COM2, and concrete and glass for COM4. Reasonable assumptions are made where input parameters are not fully specified in Arnfield (1982). Thermal parameters are based on material descriptions in Arnfield (1982) and on sources from the literature. There is no vegetation. Results are averaged over simulations with η = 0.0º, 22.5º, 45.0º and 67.5º.

Table 2: Urban land use zone case study geometric and radiative parameters.

Parameter	**COM4**	**COM2**	**RES2**	**IND**
UCZ	1	2	3	4
Geometric				
λ_p	0.36	0.25	0.17	0.48
H/L	2.00	1.25	0.57	0.13
H/W	3.00	1.25	0.40	0.29
Radiative				
α_{roof}	0.14	0.14	0.25	0.14
α_{road}	0.14	0.14	0.14	0.11
α_{wall}	0.16	0.31	0.43	0.32
ε_{roof}	0.92	0.92	0.90	0.92
ε_{road}	0.92	0.92	0.92	0.94
ε_{wall}	0.89	0.90	0.90	0.92

5. SIMULATION RESULTS

5.1 Variation of anisotropy with urban form

The June 21 dependence of the daytime maximum effective anisotropy (Λ_{max}) is plotted as a function of the geometric variables λ_p and H/L (Figure 1). Maximum daytime anisotropy is maximized for high H/L (lots of wall area) and moderate to low λ_p, which yields a balance between wall area and mutual shading of walls. Λ_{max} remains moderately high for high λ_p combined with low H/L. Effective anisotropy is maximized within a relatively narrow range of H/W (H/W ≈ 1.5-3.0 for Λ_{max}, and H/W ≈ 1.0-2.5 for Λ_{med}; Figure 2), but across a relatively wide range of H/L and λ_p (Figure 1). For $H/W > 4$ both daytime maximum and median Λ tend to level off at a moderate level of about 50-60% of the peak (Figure 2), suggesting that H/W is no longer important in producing Λ_{max} or Λ_{med} at high H/W. H/W is used instead of the more 3-D oriented wall-to-street area ratio because it is simpler and it also turns out to be more closely related to Λ_{max} and Λ_{med}(not shown).

Daytime maximum and median effective anisotropy exhibit almost identical patterns of variation

with λ_p and H/L (not shown), with Λ_{med} peaking at somewhat lower H/W by $\Delta H/W \approx -0.5$) (Figure 2), suggesting that higher H/W ratios exhibit more variable Λ and lower H/W ratios exhibit lower and more sustained daytime levels of Λ. This can also be seen in $\Lambda_{max}/\Lambda_{med}$ (Figure 2), which ranges from 1.0-1.5 when H/W is small (or very large), to 1.5-2.0 for the approximate range $1.0 < H/W < 4.0$, when the greatest diurnal variation in anisotropy might be expected.

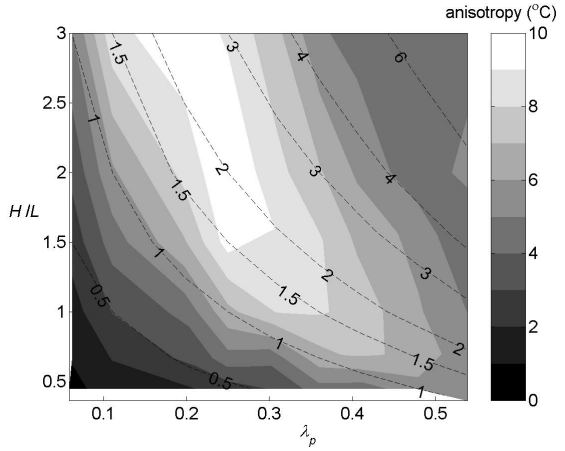

Figure 1: Daytime maximum of hourly anisotropy as a function of λ_p and H/L for regularly-spaced, aligned arrays of identical buildings with square footprints on June 21 at latitude 47º 34' N. All results are averaged over η = 0-80° in 10° increments, and interpolation is based on 9 λ_p x 6 H/L = 54 η-averaged data points. Dashed lines are lines of constant H/W.

For the geometries and the season/latitude considered here Λ_{max} and Λ_{med} are linearly related to H/W for smaller H/W and linear models are highly successful (Figure 2). These linear relations are the result of $T_{B,min}$ decreasing (as cool shaded surfaces increase due to added wall area) much more rapidly than $T_{B,max}$ with H/W.

The maximum difference from $T_{B,nad}$ (Λ_N) for the 0-45° off-nadir angle range sampled here is about 80% of Λ in the mean (or median) over all simulations during solar noon. It is higher in general for $H/W < 2.5$ and for $\lambda_p < 0.31$ given the H/L ratios sampled here, and reaches a minimum of about 60% for $H/W \approx 4.0$-5.0 (Figure 3).

5.2 Effective anisotropy of urban land use zones

The resulting diurnal trends of effective anisotropy for the four land use zones during June 21 at latitude 47º 34' N are presented in Figure 4. The character of the diurnal variation is distinctly different between the commercial (COM2 and COM4) and residential/industrial (RES2 and IND) land use zones. The former have a pronounced period of maximum effective anisotropy around midday, peaking at 1200, whereas the latter have nearly constant anisotropy from 0900 to 1500. The commercial areas also have significantly greater effective anisotropy during this midday period. Increasing H/L (and H/W) from IND to RES2 to COM2 results in increased anisotropy, and COM4 anisotropy is slightly less than that of COM2 because of mutual shading between buildings due to its higher λ_p combined with higher H/L (e.g. its H/W is greater than that for which anisotropy peaks in Figures 1 and 2). When all four land use zones have identical thermal and radiative parameters (averaged over the four land use zones) but their original geometric parameters, the results for June 21 are more or less identical ("AVG" simulations in Figure 4). This suggests that the geometric differences between the land use zones are largely responsible for the differences in simulated anisotropy. Overall, industrial and detached residential land uses exhibit less effective anisotropy than the more vertically built commercial areas. The diurnal pattern of effective anisotropy variation is quite different between the COM2/COM4 and IND/RES2 land uses as well. However, the effects of vegetation are not included in the present modeling exercise and are expected to be substantial in many detached residential areas, among other land uses.

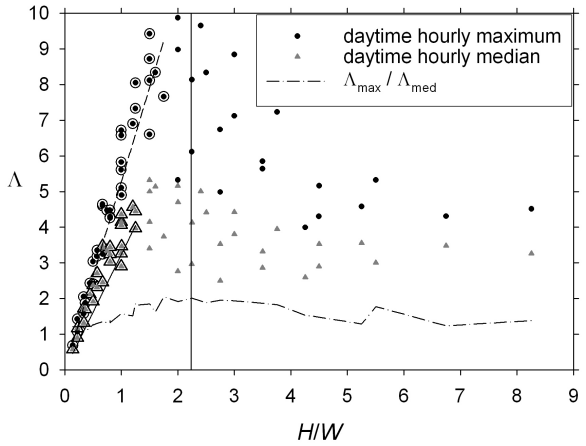

Figure 2: Daytime maximum and median of hourly anisotropy on June 21 at latitude 47º 34' N as a function of H/W for all λ_p and H/L combinations, each an average over all street orientations. $\Lambda_{med} = 3.9\ H/W$ ($R^2 = 0.83$) for $0.14 \le H/W \le 1.25$ and $\Lambda_{max} = 5.5\ H/W$ ($R^2 = 0.92$) for $0.14 \le H/W \le 1.75$, and data points included in the regression use outlined symbols. The vertical line indicates the H/W (= 2.23) whose cross-canyon elevation angle (i.e., arctan(H/W)) corresponds to the maximum solar elevation angle (65.9°) for this date.

6. CONCLUSIONS

Simulations of urban effective thermal anisotropy as observed by a narrow FOV thermal remote sensor are performed using the TUF-3D and SUM models for a range of geometrical variations of identical, aligned, equally-spaced buildings with square footprints on June 21 at latitude 47º 34' N. Within the range of simulations performed here, effective anisotropy is generally higher for greater solar elevation angle (i.e. near midday) and over a limited range of H/W (approximately 1.0 - 3.0). Furthermore, when H/W is

less than that at which effective anisotropy peaks, effective anisotropy varies linearly with *H*/*W* and the slope of this relation for daytime maximum anisotropy is ≈5.5 and for daytime median anisotropy is ≈4.0. Since the majority of urban land use zones have moderate to low *H*/*W*, this linear dependence may be useful in a practical sense. However, the effects of vegetation are not included in these relations. For large *H*/*W*, there appears to be little dependence of effective anisotropy on *H*/*W*.

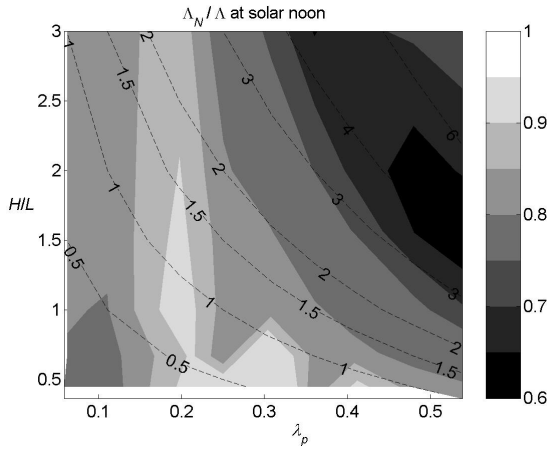

Figure 3: Maximum difference from $T_{B,nad}$ as a fraction of anisotropy, at solar noon on June 21 at latitude 47º 34' N.

The maximum difference from the nadir brightness temperature closely approximates anisotropy for most *H*/*W* with the exception of *H*/*W* > 2.5, and it is on average 80% of anisotropy in magnitude. This suggests that the use of the nadir temperature as the maximum temperature with narrow FOV sensors (e.g. Voogt and Oke, 1998) is a fairly good approximation for small and moderate *H*/*W*, but may slightly underestimate the true anisotropy.

Simulations of four urban land use zones from Arnfield (1982) provide some practical guidance for urban climatologists. Commercial zones with significant vertical structure are characterized by large daytime effective anisotropy that undergoes significant diurnal variation. High density residential and industrial areas with less vertical development yield lower anisotropy with relatively little diurnal variation.

Future work will investigate the interaction between urban form and solar geometry in the production of effective anisotropy, and the causes of effective anisotropy in terms of facet surface temperatures and sensor-facet view factors.

REFERENCES

Arnfield, A. J., 1982: An approach to the estimation of the surface radiative properties and radiation budgets of cities. *Physical Geography*, **3**, 97-122.

Krayenhoff, E. S. and Voogt J. A., 2007: A microscale three-dimensional urban energy balance model for studying surface temperatures. *Boundary-Layer Meteorol*, **123**, 433-461.

Lagouarde, J.-P., Moreau, P., Irvine, M., Bonneford, J.-M., Voogt, J. A. and Solliec, F., 2004: Airborne experimental measurements of the angular variations in surface temperature over urban areas: case study of Marseille (France). *Remote Sens Environ*, **93**, 443-462.

Mills, G., 1997: An urban canopy-layer climate model. *Theor Appl Climatol*, **57**, 229–244.

Oke, T. R.: 2006: Towards better scientific communication in urban climate. *Theor Appl Climatol*, **84**, 179-190.

Soux A., Voogt J. A., Oke T. R., 2004: A model to calculate what a remote sensor 'sees' of an urban surface. *Boundary-Layer Meteorol*, **112**, 109–132.

Voogt, J. A., and Krayenhoff, E. S., 2005: Modeling urban thermal anisotropy', *Proc. 5th International Symposium Remote Sensing of Urban Areas*, Phoenix, AZ (CDROM).

Voogt, J. A., Oke, T. R., 1998: Effects of urban surface geometry on remotely sensed surface temperature. *Int J Remote Sens*, **19**, 895–920.

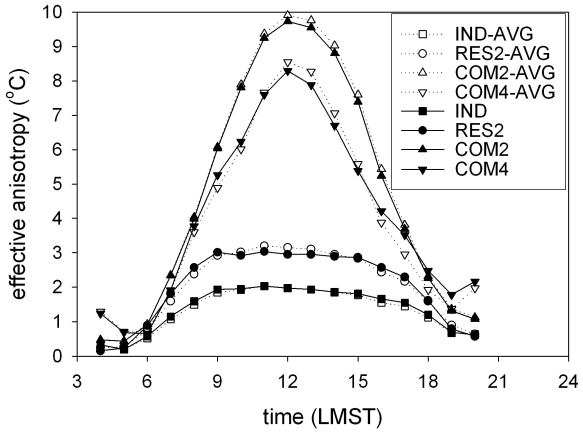

Figure 4: Diurnal variation of effective anisotropy for four urban land use zones based on Arnfield (1982) on June 21 at latitude 47º 34' N, each averaged over η = 0.0, 22.5, 45.0, and 67.5. "AVG" simulations all use identical thermal and radiative parameters, but their original geometric parameters (see Table 2).